BACHELOR' S THESIS / BIOMEDICAL ENGINEERING 2023

On the basis of impaired functional connectivity in psychosis: the role of structural substrate and neurometabolites contribution

Nerea González Aranceta

upf. Universitat Pompeu Fabra Barcelona

On the basis of impaired functional connectivity in psychosis: the role of structural substrate and neurometabolites contribution

Nerea González Aranceta

Bachelor's Thesis UPF 2022/3

Thesis Supervisors:

Mireia Masias i Bruns, (Department of Information and Communication Technologies, UPF)

Dr. Gemma Piella Fenoy, (Department of Information and Communication Technologies, UPF)

upf. Universitat Pompeu Fabra Barcelona

upf. Universitat Pompeu Fabra Barcelona

Universitat Pompeu Fabra Barcelona

Acknowledgments

I would like to profoundly thank my supervisors, Mireia Masias and Gemma Piella for o□ering their help and guidance throughout the project.

In addition, I want to acknowledge the paper my family and friends have played in the development of the project by supporting and encouraging me in these past few months.

Abstract

Psychotic disorders are characterized by the presence of symptoms related to a distortion of one's perception of reality. In its early stages (First Episode of Psychosis, FEP), patients may show diffuse symptomatology that lays in a spectrum delimited by bipolarity and schizophrenia on both ends. Some studies point to a disconnection of the brain as a network as the most likely cause of the symptoms of the disease. Functional connectivity (FC) arises from the interaction of neurometabolites and a structural substrate, and inferring the contribution of each of these elements is not possible using traditional approaches. Accordingly, we aimed to explore the structural connectivity and use of simulations to infer the synaptic contribution of the emerging FC in FEP patients. First, structural connectivity from diffusion-weighted images was obtained and compared between Healthy Controls (HC), Affective Psychoses (AF), and Schizophrenia Spectrum Disorders. Second, synaptic-level properties, such as global connectivity, were inferred per subject based on Hopf-Bifurcation by selecting the parameters that produce the closest FC simulated to the experimental FC. Finally, a comparison of the extracted measures between the three groups was performed. The obtained results showed differences in the substrate of the three groups, with AF being the one with larger disparities from HC. As for the simulations, there were no differences for the global connectivities that generated the most accurate representation; however, for AF the similarity of the simulated static FC was lower to experimental static FC, which could suggest a higher neurometabolic contribution for this group.

Keywords

First Episode of Psychosis, structural connectivity, synaptic-scale properties, resting-state fMRI, Hopf bifurcation model

Preface or prologue

The effects that psychosis has on the brain have been long studied, and a disconnection of the brain as a network has been recognised in chronic stages of the disease. However, it is not yet clear which are the causes of its symptomatology. Some studies point to this disconnection as the most likely cause. It seems reasonable, thus, to analyse the functional connectivity (FC) in the early stages of the disease, when the non-causal brain alterations may be not yet developed. In fact, differential alterations have already been reported in clinical First Episode Psychosis (FEP) subgroups. One of the most accepted hypotheses regarding the etiopathogenesis of psychosis, partially supported by experimental findings, is that neurometabolites dysfunction might be the primary cause of FC impairments, which are responsible for subsequent structural connectivity alterations. Consequently, this project aims to explore the contribution of the structural substrate and neurometabolites in the development of the disease in hopes of disclosing their cause-consequence relationships with the disease.

Universitat Pompeu Fabra Barcelona

Index

List of Figures

List of Tables

1 Introduction

1.1 Psychosis

Psychosis is a psychopathological condition, characterized by the development of positive (i.e. delusions and hallucinations), negative (i.e. apathy and reduction in the emotional expression) and/or cognitive (i.e. deficits in memory, attention and problem-solving) impairments. Such a condition encompasses a spectrum of diseases with shared symptomatology in a spectrum delimited by schizophrenia and bipolar disorders on both ends [1].

The causal mechanisms of psychosis are yet unknown. However, multiple plausible hypotheses have been proposed in the literature. Generally speaking, and long supported by neuroimaging studies [2], it is thought that a disconnectivity state of the brain underlies such diseases and that such a disconnectivity state can be mechanistically explained from two different perspectives. First, due to an aberrant substrate or structural disconnection; and second, due to a neurotransmission failure, caused either by the presence of aberrant neurotransmitters or by the malfunction of their receptors, meaning a functional disconnection.

The disconnection hypothesis, proposed by Firston and Frith (1995) [3] and Weinberger (1993) [4], supports a functional disconnection on its origin and links such mechanistic processes to the onset of psychotic symptoms. The authors in [5] interpret the onset of positive symptoms in terms of disturbance of normal inference mechanisms of the brain, in the last instance caused by brain network disconnections, involving key brain regions (i.e. thalamus, limbic system structures and prefrontal cortex) [2, 6].

In a typical process, the brain is constantly making predictions about its surroundings that are reliant on prior knowledge of expectations, which are learnt causes for diverse received sensory inputs. These predictions are generated in higher levels of cortical hierarchies (deep pyramidal cells) based on the sensory input stored in the lower levels (superficial pyramidal cells), which is the brain's information about reality. Then, the generated predictions are compared to the sensory input. With this comparison, the lower levels are able to encode a prediction error that the brain tries to minimize by modifying the expectations. When this error is minimised, the brain is able to give its best explanation, or inference, to the sensory inputs received. Each time, the brain learns to make more accurate predictions for the future. According to this hypothesis, positive symptoms suffered by the patients could be explained by a failure in the inference process. In this case, the brain is unable to minimize the prediction errors, which implies the predictions could be prone to distancing from reality. As the prediction error is generated through the comparison of both the predicted and received information, any kind of disconnection involving the mainly responsible regions could explain the inability of error minimization by the brain, and thus, the generation of false sensory perceptions by reducing the sensory precision [5].

1.2 Disconnection mechanisms

As previously stated, both structural and functional disconnectivities have been long reported in the clinical literature in patients with distinct symptomatologies within the psychosis spectrum [2], and while they are typically jointly observed in chronic adult patients, [5] justifies that there is a larger probability for the disease to display a synaptic pathophysiological causal mechanism in the first instance, being responsible for a subsequent structural disconnection.

Several synaptic (sub)hypotheses have been proposed in the literature, requiring further investigations [5, 7]. However, physiological hypofunction in the NMDA receptor (NMDAr) system, which is responsible for synaptic plasticity and cognitive functions such as memory and learning [8], has been identified as a possible cause of psychosis. While it is not confirmed that this is the reason after functional disconnectivity, there is increasing evidence that suggests a possible link between NMDAr action is synaptic plasticity and the amount of prediction error signal generated [8].

The dysfunction in the NMDAr system may provide a potential explanation for the functional connectivity deficits and the link to structural deficits, through the loss of excitation-inhibition balance, as seen in Figure 1.

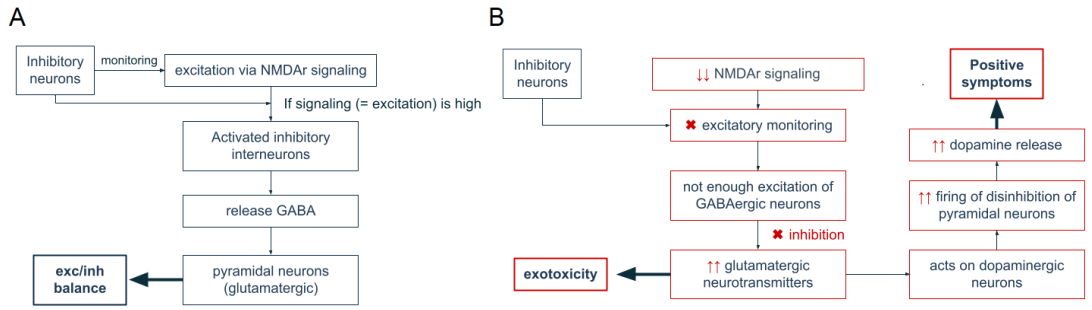

Figure 1: A: Representation of the normal processes that maintain excitation-inhibition balance. B: Representation of the hypofunction of the NMDAr and its consequences.

In a typical context, NMDArs activate in the presence of glutamate, which is an excitatory neurotransmitter. When NMDArs signal the presence of glutamate, the inhibitory neurons or interneurons, which moderate the excitation of neurotransmission, are activated, and they release the inhibitory neurotransmitter GABA. GABA in its turn inhibits the pyramidal neurons, which are responsible for glutamate release, and thus the excitation-inhibition balance is kept [9].

When a hypofunction of the NMDArs is present, a decrease in NMDAr signalling is experienced, which means that the inhibitory neurons are no longer able to monitor the excitation of neurotransmission. Then, GABA is not released, and compensatory inhibition does not happen. Therefore, the concentration of glutamatergic neurotransmitters does not stop increasing. This may have two main consequences. Firstly, large glutamate concentrations in brain regions lead to an exotoxicity in the brain, responsible for neuronal loss, which has been long reported in the clinical

literature [6, 10, 11]. Secondly, this might have an effect on dopaminergic neurons, which become overly activated and release a greater amount of dopamine to the brain. This excessive dopamine is related to the positive symptoms present in psychosis [9]. Moreover, there are plausible mechanisms that can explain structural disconnection from such synaptic alterations (e.g. via activity-dependent pruning), while the inverse is less obvious. However, further experimental research is required to disentangle cause-consequence relationships. This is where the study of populations at the onset of the disease becomes interesting.

1.3 First Episode Psychosis

As previously introduced, the analysis of samples at the initial phases of the disease, before the effects of chronicity and protracted exposure to antipsychotic treatment is of special interest. This might be the case for Early Onset First Episode of Psychosis (FEP), a non-chronic stage of the disease in which a person first experiences symptoms of losing touch with reality [12]. The likelihood of recurrence is higher for patients between the ages of late teens to mid-twenties [13]. When it occurs, the prognosis can largely vary, and symptoms may be specific, being patients at risk of experiencing psychosis at any point on the spectrum. Over time, patients who transition to psychosis can be subsequently classified into two groups according to DSM-V: affective and non-affective. Affective FEP is characterized by changes in mood and is closer to the bipolar disorder extreme on the spectrum, including bipolarity. Non-affective FEP, on the other hand, does not present mood alterations and is closer to the schizophrenia extreme on the spectrum [14].

1.4 Objective and hypotheses

The aim of this study is to analyze and characterize both structural and functional connectivity in the resting-state functional magnetic resonance (rs-fMRI) in an early-onset FEP population, which could explain the altered biomarkers found especially and further shed light on the aetiopathogenesis of the disease. These differences could be explained by either an aberrant substrate, by alterations at the synaptic level, or by the interaction between the two.

To do so, we will first compare the structural connectivity (SC) obtained from DTI preprocessing of three distinct populations, healthy controls (HC), affective FEP (AF), and non-affective FEP or schizophrenia spectrum disorder (SSD). Then, we will simulate the functional connectivity using generative brain models based on the structural substrate and neuronal population activity interaction, and finally perform parameter inference between the three groups.

On the assumption that the previously explained psychological and physiological mechanisms are accurate, it has been found a functional disconnection in the non-affective population that is not present in the affective group [15]. Based on this, we expect to observe affected functional connectivity in the non-affective group when studying the global connectivity in the connectivity matrices, and possibly some compensatory mechanisms in the affective group. However, considering Firston's

theory that structural connectivity is a consequence of the disease, we do not expect it to necessarily be altered between these two groups in such early stages.

2 Methods

2.1 Data

For this study we used T1-weighted magnetic resonance (T1w) images, Diffusion-weighted imaging (DWI), and rs-fMRI data from 133 patients aged 10-17, scanned at first contact with hospital due to a first episode of psychosis, at a 3T Siemens scanner. Recruited patients showed a disease duration of less than a year. Patients were further divided into two different groups, according to confirmed diagnoses at 6 months follow-up into affective FEP (n=43) and non-affective FEP (n=36). Age and sex-paired healthy volunteers (n=51) were recruited from the same geographical area. There was no significant age difference between the groups, although there was a difference in the distribution of sex, with 60.50% female in AF and 41.70% female in SSD. The global intelligence quotient differed in the three groups, with significantly higher scores in HC than the rest, and higher for AF than SSD, however, this parameter had no significant difference between the patient groups (p-value = 0.267). Cannabis use had more prevalence in the SSD group (30.60%) than AF (14.00%), while the difference in antipsychotic doses between the patient groups (SSD and AF) was not significant (p-value = 0.281). All the images were obtained at the Department of Child and Adolescent Psychiatry and Psychology of the Hospital Clínic of Barcelona (Spain). The demographic information on the data is shown in Table 1.

	HC	**SSD**	**AF**	**p-value**
	N = 51	N = 36	N = 43	
Age	15.6 (2.54)	15.4 (1.85)	15.2 (1.34)	0.597
Sex:				0.238
Male	26 (51.0%)	21 (58.3%)	17 (39.5%)	
Female	25 (49.0%)	15 (41.7%)	26 (60.5%)	
Scan:				0.193
Trio	38 (74.5%)	29 (80.6%)	27 (62.8%)	
Prisma	13 (25.5%)	7 (19.4%)	16 (37.2%)	
Cannabis:				0.083
None	40 (87.0%)	25 (69.4%)	37 (86.0%)	
Use	6 (13.0%)	11 (30.6%)	6 (14.0%)	
IQ	105 (12.7)	85.1 (20.4)	89.9 (16.2)	<0.001
ATP dosage	0 (0)	255 (207)	330 (330)	<0.001

Table 1: Demographic information of the data used in this study.

2.2 Structural connectivity

Diffusion magnetic resonance imaging (MRI)-based tractography is the standard chosen protocol for the derivation of structural connectivity matrices. These matrices depict the strength of the connections between different brain regions based on the structural substrate, or anatomical paths, which are assumed to occur in the same direction in which myelinated axons are oriented. In order to obtain the final structural connectivity matrices, DWI images needed to be preprocessed to ensure the quality of the scans, and finally turned into Diffusion Tensor Imaging (DTI). The overall pipeline is summarized in Figure 2 and is further explained in the next sections.

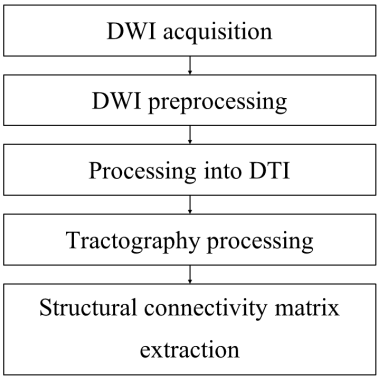

Figure 2: Pipeline of extraction of structural connectivity.

2.2.1 DWI preprocessing

For the preprocessing, we applied a pipeline previously implemented in the research group, which is in accordance with the pipeline proposed by ENIGMA [16]. The pipeline consists of, first, the reorientation to the standard position of the images, which was accomplished with FSL's [17] *fslreorient2std*. Then, skull stripping was performed, in which the skull and other tissues not related to the brain were removed with *Advanced Normalization Tools* (ANTs) [18] and using the mask provided by *The pediatric template of brain perfusion* (PTBP) [19]. Since the DWI acquisitions contained 30 gradient direction orientations, each subject's 3D images were stored in the same 4D file. The resulting image was denoised in order to remove the thermal noise generated during the MRI acquisition, using the *DWIDenoise* function from *Mrtrix3* library [20]. After that, we performed a DWI bias field correction with *Mrtrix3*'s *DWIBiasCorrect* to reduce the inhomogeneities from the magnetic field. Finally, with FSL's function *eddy_correct* eddy currents and motion corrections were performed to maximize the signal-to-noise ratio of the images, as well as the contrast-to-noise ratio.

2.2.2 Diffusion Tensor Imaging

After preprocessing, the extraction of the DTI was possible. The tractography was obtained using *Mrtrix3*'s *tckgen* tool, using a deterministic approach from the func-

tion *Tensor_Det*. Deterministic techniques are considered less accurate for tractography computation when compared to probabilistic techniques. The main reason is that deterministic approaches do not have the ability to account for crossing fibres, so only main directions are kept in the final model. However, in a previous analysis of the group it was determined that deterministic models o□er the best trade-o□ between computational costs and the quality of the generated connectivity matrices. Moreover, Sarwar and colleagues [21] have recently reported the advantage of multi-fibre deterministic models over probabilistic ones regarding the avoidance of false-positive connections. For all the aforementioned, in the present study, we conducted a multi-fibre deterministic approach.

For the construction of connectivity matrices, *Tensor_Det* requires segmentation of the brain into di□erent regions of interest (ROIs). For this end we used *FreeSurfer* to segment each subject's T1-weighted brain images into discrete ROIs, using the Desikan-Killiany atlas, so that parcellation and segmentation of cortical and subcortical structures were achieved. Using each patient's parcellation and tractography, an 84x84 undirected connectivity matrix was obtained per patient, by computing the number of streamlines between each pair of ROIs. See Additional information A1 to see the regions included.

2.2.3 Structural connectivity comparison

In order to compare the structural connectivity between the three groups, we propose to use a Graph Theory approach. In this methodology, brain connections are studied as networks, in which the nodes are regions and are connected by edges, representing the structural strength of connections or the number of fibres between them.

This method enables the analysis of whole-brain structural connectivity from the derived connectivity matrices by computing some standard summary measures, reflecting di□erent connectivity properties. For this analysis, the *Brain Connectivity Toolbox* [22] was used. Particularly, the analyzed global graph measures were:

- **Characteristic path length (CPL):** it measures the average for all pairs of edges in a network of the minimum number of edges that have to be transited in order to get from one node to another. CPL is an integration measure that quantifies the potential for information transmission, and a shorter CPL means that information is able to spread faster through the network. The issue with CPL is that in matrices deemed as disconnected, the value assigned to CPL is infinite, which means that in these cases, CPL may not be o□ering meaningful enough information about the network.
- **Global efficiency (EGLOB):** it represents the travelling speed of information through the network. This measure is roughly the inverse of CPL, however, it is relevant to study this measure, as it can quantify more precisely than CPL in networks deemed as disconnected. Both CPL and EGLOB of structural brain networks have been related to the performance in intelligence tests.
- **Mean clustering coefficient (MCC):** it computes the average of each

node's neighbours' connectivity to each other in proportion to the maximum number of connections in the network. It is a segregation measure.

- **Small-worldness (SW):** A network presents SW characteristics when it has high MCC and short CPL in comparison to randomly generated networks of the same size. When this happens, the network is able to transmit information within itself with great effectiveness.

As previously stated, we initially hypothesized that in the early stages of the disease, structural disconnectivity has not been significantly developed yet. Thus we expected these measures to be preserved in patients with respect to controls. To test this, first, the distribution of parameters was visualized. Whenever the network parameters followed a normal distribution, an analysis of variance (ANOVA) was performed for each measure per group, using as covariates the patient's age, sex, scan used for image acquisition, cannabis use, and antipsychotic treatment doses. Whenever the normality assumption was not met, the Kruskal-Wallis test was performed, being a non-parametric ANOVA alternative (i.e., no assumptions are made regarding the probability distribution of data). The p-values obtained per experiment were corrected to account for multiple comparisons using false discovery rate (FDR) correction. A difference between groups was considered significant whenever the p-value was lower than 0.05.

2.3 Functional connectivity

Static Functional Connectivity (sFC) was derived from the blood-oxygenation-level-dependent (BOLD) time series, acquired in a 3T scanner, with a repetition time (TR) = 2 s and 240 time points. The derivation of sFC relies on the idea that functionally connected regions should co-vary similarly [23]. However, the rs-fMRI signal is subjected to a considerable amount of noise and artifacts, for which preliminary preprocessing is of paramount importance. Although the final experimental sFC was already provided, in this section we will provide the steps followed for reproducibility purposes.

2.3.1 Rs-fMRI preprocessing

The preprocessing protocol used was based on guidelines provided by [24]. Shortly, the first four volumes were excluded while the rest were merged into a single 4D file image which was slice time corrected. Each slice was then realigned, first to the first volume and then to the mean of them. In order to correct for EPI distortions, both the T1w reference image and rs-fMRI were skull-stripped, and the T1w image and its associated *FreeSurfer* segmentation were re-sliced to rs-fMRI space. The mean rs-fMRI volume was then registered to the reference T1w image, using rigid, affine, and non-linear transforms. The estimation of the required transformation was then applied to the rest of the rs-fMRI volumes. Finally, linear detrending, intensity normalization to mode 1000 unit, and spatial smoothing using a 6mm FWHM, and a band-pass Butterworth filter, of order 4, within the frequency range [0.0008, 0.008] Hz was applied on the rs-fMRI signal.

2.3.2 sFC acquisition

As previously stated, the basic idea behind sFC is that functionally connected regions should co-vary similarly. Therefore, in order to construct the sFC matrix per subject, ROI-to-ROI association was obtained by computing the correlation between the mean temporal signal from both ROIs of interest. An example of the experimental sFC is shown in Figure 3.

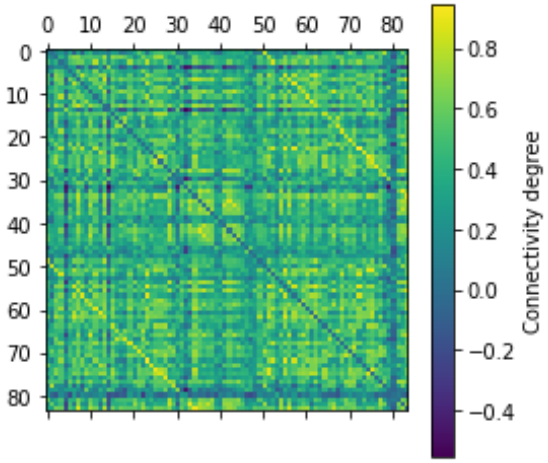

Figure 3: Experimental sFC from rs-fMRI of a HC.

2.4 Simulations

Once the structural connectivity was explored, in this second part of the project we aimed to approximate the neurometabolic and structural contribution in the sFC. For this aim, we tried to approximate it by means of generative computational models. Several models were explored and evaluated in terms of computational e□ciency, similarity to the experimental sFC, and significance of the basal parameters to be explored regarding our clinical question.

Several models were explored. In the upcoming subsections, we will introduce the evaluated models and show some of the performed simulations. The final selected model is described in detail, as well as our data-driven method to define the optimal number of simulations to average in order to obtain robust enough results. We will explain the inference of parameters, and the statistical analysis to compare the extracted basal parameters between di□erent groups as well.

2.4.1 Models

For the simulation of the functional connectivity, we finally applied a Hopf bifurcation model based on [25]. This model describes local node neural mass dynamics, in which the behaviour described as BOLD signals of a large number of neurons with similar dynamics, is described as a single node. This way, the brain is described as a network of individual groups of neurons interacting.

In order to emulate the activity of the different neuron populations, this model combines the dynamics of Stuart-Landau oscillators, and noisy asynchronous dynamics in order to simulate the resting state activity fluctuations of different regions in the brain.

The first part of this model, the Stuart-Landau oscillators, describes the dynamics of each component of the system as a normal form of a Hopf bifurcation. In this case, the Hopf bifurcation is supercritical, which means that the values that arise before the bifurcation have a lineal-stable behaviour, whereas those greater than this parameter begin to oscillate [26].

The noise added to this oscillation is in this case Gaussian noise. This kind of noise presents random independent fluctuations that are described by a probability density function that follows a normal distribution. This kind of noise, when added to a dynamical system as a source of variability, can make the system's individual components act in an asynchronous manner with respect to the rest.

Thus, the whole-brain dynamics are described with equations 1 and 2, in which x and y are respectively the real and imaginary parts of the dynamics of region j being computed, a refers to the bifurcation parameter, ω is the intrinsic frequency of region j, G the global coupling, C_{ij} is the structural connectivity of the region j to the other regions i, and $\eta_j(t)$ is the added Gaussian noise, with standard deviation β.

$$\frac{dx_j}{dt} = [a_j - x_j^2 - y_j^2]x_j - \omega_j y_j + G \sum_i C_{ij}(x_i - x_j)\beta\eta_j(t) \quad (1)$$

$$\frac{dy_j}{dt} = [a_j - x_j^2 - y_j^2]y_j + \omega_j x_j + G \sum_i C_{ij}(y_i - y_j)\beta\eta_j(t) \quad (2)$$

The parameters of interest in this model that can be modified are the global coupling factor (G) and the bifurcation values. G defines the degree to which the functional dynamics of the brain are dependent on structural connectivity. As previously mentioned, the structural connectivity of the brain represents the way the substrate of the brain is organized, while the functional connectivity is related to the functioning of the neurometabolites, thus functional connectivity is dependent on the structural one to a certain degree. Since we want to study the contribution of each connectivity across the subjects' populations, this is the parameter that we modified to study. The bifurcation parameter defines at which point the system turns from stable to an oscillation, and vice-versa. However, this parameter was not modified in this study, and the found optimal value for it in [25], at -0.2, was kept constant.

In order to generate the simulations, the needed information by the model was the structural connectivity matrices extracted in section 2.2, and the intrinsic frequency for each ROI. The acquisition of the latest is explained in the following section.

2.4.2 Intrinsic frequencies

The intrinsic frequency in this case refers to the frequency that predominates in the BOLD signals from the rs-fMRI for each ROI (see Additional information A1). In order to extract the mean temporal signal per ROI, we projected the previously segmented T1w images with *Freesurfer*, resized to the rs-fMRI resolution, on top of the preprocessed rs-fMRI images. The temporal signal for each ROI was then obtained by computing the average of the temporal signal sequences across all pixels within each ROI. A Fourier transform was then applied to obtain the frequency spectrum, from which we could subsequently identify the highest peak within it. The location of this peak corresponded to the dominant frequency, which was stored and considered as the intrinsic frequency for the corresponding ROI.

2.4.3 Number of repetitions

As previously mentioned, rs-fMRI simulations partially depend on random noise, as experimental rs-fMRI do. We can either generate several repetitions of a specific simulation and/or acquire several rs-fMRI sequences of the same subject. Even though the latter is not possible, we could easily amend the first condition. Nonetheless, the optimal number of repetitions remains unknown. Therefore, we proposed to determine the ideal number of repetitions, in terms of cost-e□ciency, in a data-driven manner.

Our hypothesis was that by adding up consecutive simulated sFC, we would reach a point from which the mean of all simulated sFC would not significantly change anymore, reaching a plateau. Consequently, in order to determine the minimum number of repetitions required, we first generated 20 repetitions with the same parameters. Then, we computed the Pearson correlation of the obtained mean matrices between increasing number of repetitions (i.e. the result of the first simulation vs. the mean of the first two, then the latter vs the mean of the first three...), getting the plot displayed in Figure 4.

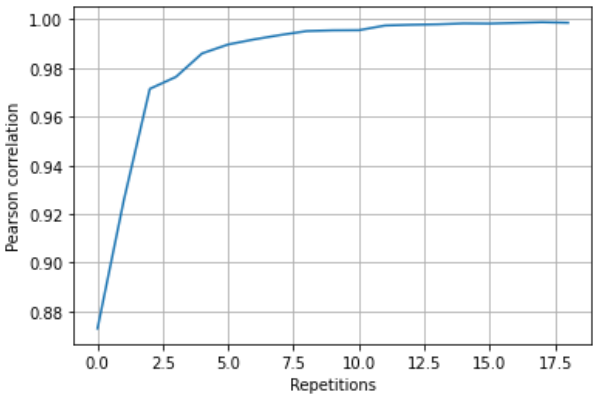

Figure 4: Correlation plot of mean sFC to determine the minimum required number of repetitions for the Hopf bifurcation model simulations.

As expected, the correlation curve followed a saturation curve, from which we could determine that it is not until the fifth repetition that the Pearson correlation reduces

significantly its increasing rate. Considering that it is significantly high at this point, for the sake of computation time optimisation, this was the number of repetitions we chose for our subsequent experiments.

2.4.4 Synaptic parameters inference

Once structural connectivity and intrinsic frequencies had been defined per patient and ROIs, we ran the simulations described in section 2.4.1, the number of times defined in section 2.4.3, for a specific value of the parameter of interest, in this case, the G, which explains the contribution of the structural connectivity in the prediction. The basic idea was to identify the associated G that could best approximate the simulated sFC to the experimental one. The peak correlation at this point could also provide relevant information, as in preliminary results we observed that the peak correlation could vary across subjects when the bifurcation parameter is kept constant across all ROIs. Therefore, a ratio of $G/Corr_{Peak}$ was also computed as a normalized G measure.

Accordingly, we performed the simulations varying the parameter G, from 0.25 to 10, with increasing steps of 0.25. We performed 5 repetitions for each patient and G value, which amounted to a total of 40 simulations per patient. The generated result of applying this model was the simulated BOLD time series signals per ROI, from which the simulated sFC could be computed as we did for the experimental sFC: each ROI-to-ROI interaction was computed as the correlation between simulated time-signals. Each resulting simulated sFC was compared to the experimental one through the computation of the Pearson correlation coe□cient.

Some instances of the Pearson correlation per subject and G are shown in Figure 5. These preliminary results suggest that even though 5 repetitions allowed to produce roughly robust results, with a clear $G - Corr_{peak}$ curve, residual variation remained. In order to overcome this limitation and to approximate the exact G value from a limited set of simulations, we adjusted a third-order curve using the least squares method. This assumption was made to avoid over-fitting while enabling the analytical identification of a first local maximum or a saddle point in the absence of the former.

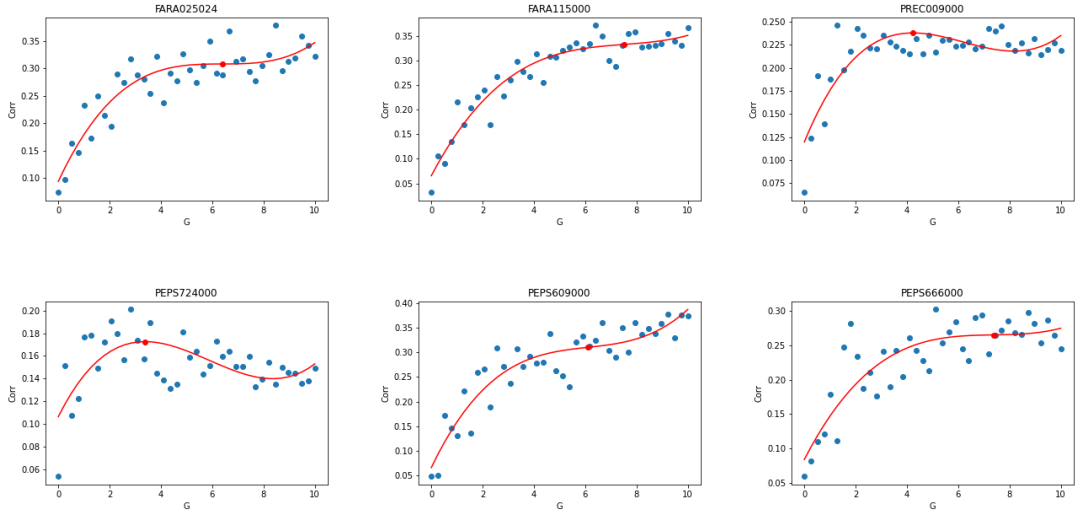

Figure 5: Examples of the G/Corr curves. Top three: healthy individuals, and the bottom three: FEP patients.

Based on the experimental observation of the results, they happen between the growth phase and the subsequent stabilization of the correlation. Therefore, for each individual, a third-order polynomial was fitted into its correlation values. To find the first local maximum of the obtained curve, the derivative of the curve was computed and equalized to zero in order to find the abscissa values (Gs) corresponding to the local maxima. Whenever there was a solution for this second-order equation, the lower found G was selected. When no real solution existed for the equation, the second derivative was equalized to zero in order to find the G-value corresponding to the saddle point of the curve.

Finally, the found G-value, its corresponding Pearson correlation and the ratio between the two were stored.

2.4.5 Statistical analysis

As we did for the statistical analysis in section 2.2.3, ANOVA was performed on the obtained measures (G, correlation and G/correlation ratio) whenever the normal distribution assumption was met. Otherwise, the non-parametric alternative, the Kruskal-Wallis test, was applied. Then, the p-values obtained per experiment were corrected with post hoc non-parametric test Dunn's Multiple Comparison Test using FDR correction, considering a difference between groups significant whenever the p-value was lower than 0.05.

3 Results

3.1 Structural connectivity

Structural connectivity matrices were computed as stated in section 2.2. For visualization purposes, the mean structural connectivity matrix is shown in Figure 6.

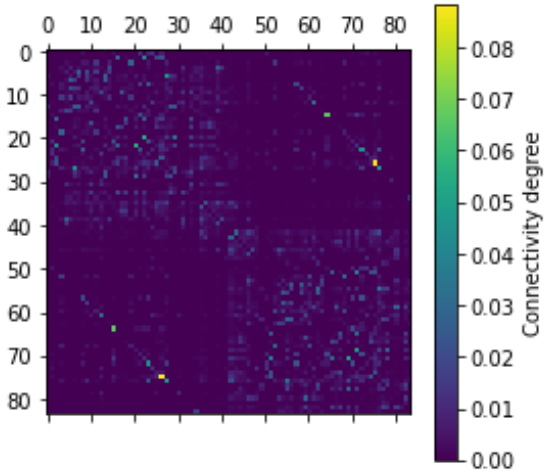

Figure 6: Mean connectivity of all obtained structural connectivity matrices. Each row and column index corresponds to the specified in Additional information A1.

Then, the distributional normality assumption was then assessed. Group distributions did not meet normality criteria for any of the tested measures, as seen in Figure 7. Consequently, the Kruskal-Wallis test was used instead of ANOVA.

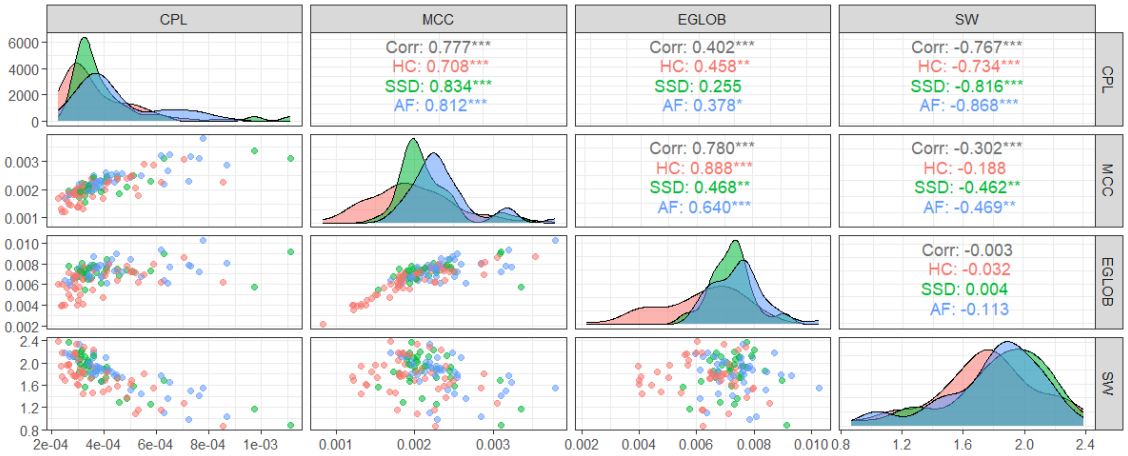

Figure 7: Distribution of populations.

The results of the Kruskal-Wallis test, after multiple pairwise comparisons correction, are presented in this section. First, the boxplot results of the Kruskal-Wallis test are portrayed in Figure 8, along with the general result values for each measure.

Then, for each measure, the mean and standard deviation of each group are shown in Table 2.

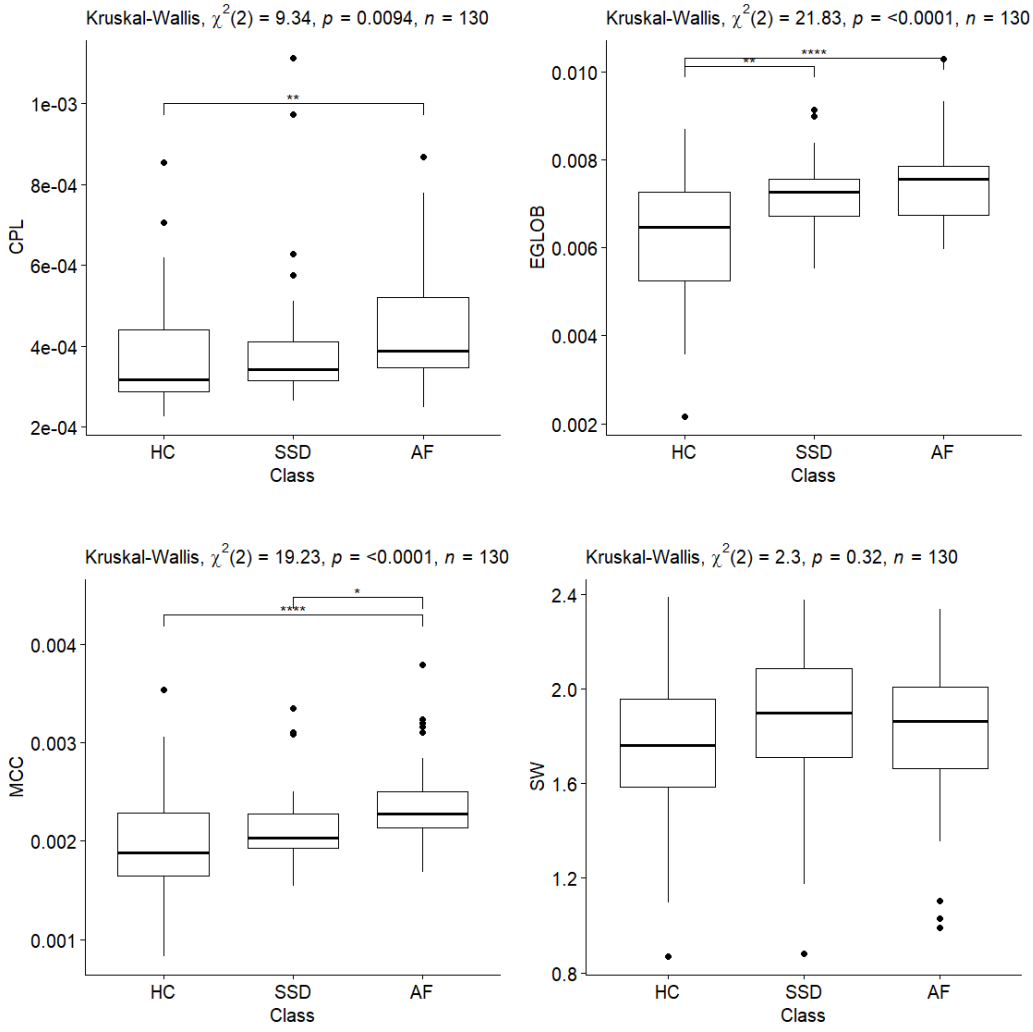

Figure 8: Measures obtained during the Kruskal-Wallis test for each group.

	HC	SSD	AF	p-value	Post hoc
CPL	3.74×10^{-4} (1.35×10^{-4})	4.08×10^{-4} (1.79×10^{-4})	4.51×10^{-4} (1.61×10^{-4})	9.361×10^{-3}	HC<AF**
EGLOB	6.18×10^{-3} (1.46×10^{-3})	7.21×10^{-3} (7.56×10^{-4})	7.46×10^{-3} (9.13×10^{-4})	6.685×10^{-5}	HC<AF**** HC<SSD**
MCC	1.96×10^{-3} (5.34×10^{-4})	2.16×10^{-3} (3.83×10^{-4})	2.36×10^{-3} (4.26×10^{-4})	1.816×10^{-5}	HC<AF**** SSD<AF*
SW	1.76 (3.36×10^{-1})	1.84 (3.31×10^{-1})	1.80 (3.19×10^{-1})	0.3164	ns

Table 2: For the results obtained in the statistical analysis of CPL, EGLOB, MCC and SW: means and standard deviations for each group (HC, SSD and AF), p-value obtained for the Kruskal-Wallis test, and significance found after Dunn's post hoc test.
*: $0.06 >$ p-value $>= 0.01$, **: $0.01 >$ p-value $>= 0.001$, ***: $0.001 >$ p-value $>= 0.0001$, ****: $0.0001 >$ p-value $>= 0$, no-significance (ns): p-value $>= 0.06$.

As shown in Table 2 and Figure 8, only EGLOB and MCC appear to be significantly different across the three groups. In both first measures, the greatest difference was found between HC and AF, where AF showed greater EGLOB and MCC when compared to HC. Moreover, there was a significant difference between SSD and HC, and SSD and AF in measures EGLOB and MCC, respectively.

There is also a significant difference between HC and AF in the measure CPL, in which AF presents larger values than HC. However, SSD is not significantly different from the other groups for this measure. Finally, SW presents no meaningful differences between the three populations.

It is worth noting that while images were being acquired, a scanner upgrade was performed. Although the vendor and intensity field were the same, this could lead to potential differences in the connectivity matrices not related to the class. Although we did not find statistically significant differences in the scanner used per group (see Table 1), we repeated the experiments only using the most prevalent scanner, to confirm the previous results. In Figure 9, the same tests are shown only with the patients whose images were obtained with the most common scan.

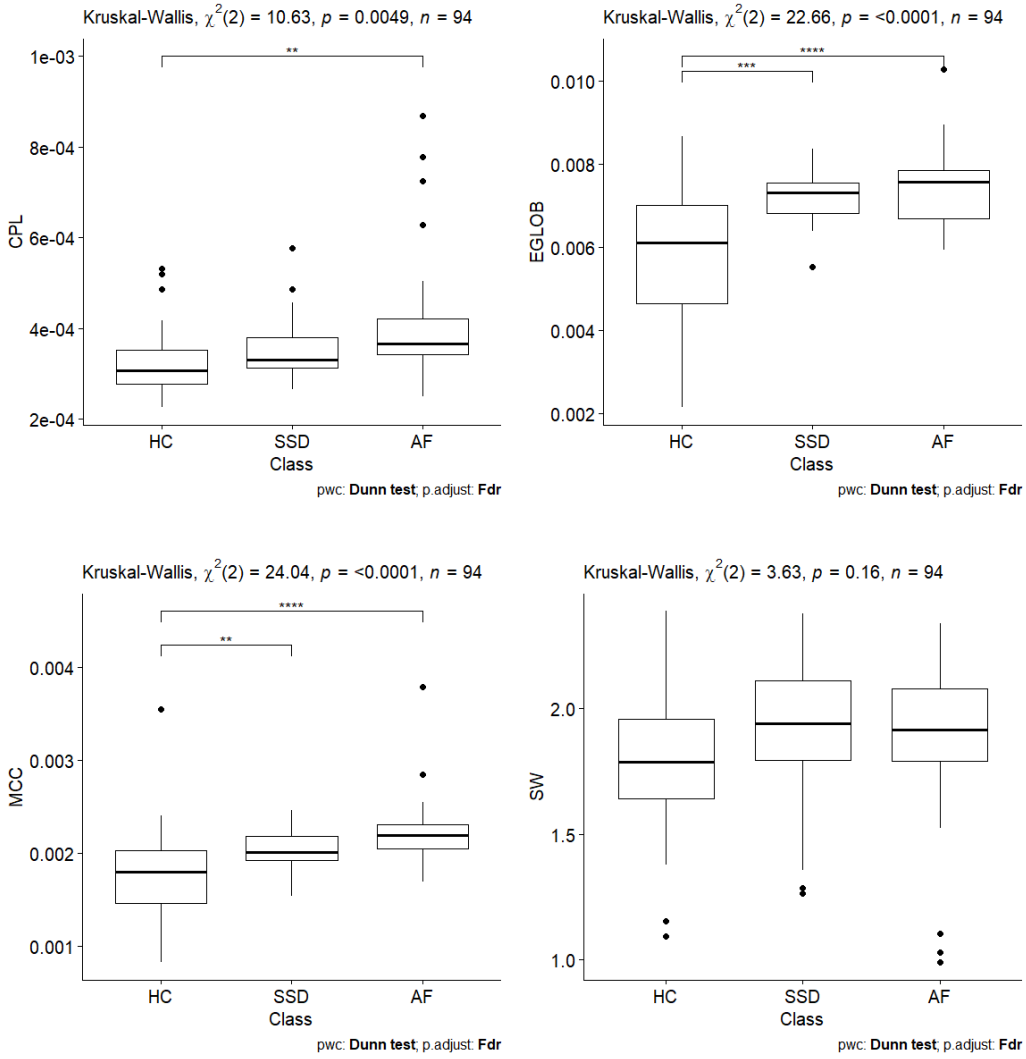

Figure 9: For images with Trio scan, measures obtained during the Kruskal-Wallis test for each group.

	HC	SSD	AF	p-value	Post hoc
CPL	3.24×10^{-4} (0.77×10^{-4})	3.55×10^{-4} (0.70×10^{-4})	4.15×10^{-4} (1.60×10^{-4})	4.91×10^{-3}	HC<AF**
EGLOB	5.88×10^{-3} (1.50×10^{-3})	7.19×10^{-3} (5.76×10^{-4})	7.47×10^{-3} (9.78×10^{-4})	1.20×10^{-5}	HC<AF**** HC<SSD***
MCC	1.79×10^{-3} (4.71×10^{-4})	2.05×10^{-3} (2.24×10^{-4})	2.24×10^{-3} (3.98×10^{-4})	6.02×10^{-6}	HC<AF**** HC<SSD**
SW	1.79 (2.99×10^{-1})	1.90 (2.78×10^{-1})	1.84 (3.51×10^{-1})	1.63×10^{-1}	ns

Table 3: For the results obtained in the statistical analysis of CPL, EGLOB, MCC and SW, with only the data extracted from the most common scan (Trio): mean and standard deviations for each group (HC, SSD and AF), p-value obtained for the Kruskal-Wallis test, and significance found after Dunn's post hoc test.
*: $0.06 >$ p-value $>= 0.01$, **: $0.01 >$ p-value $>= 0.001$, ***: $0.001 >$ p-value $>= 0.0001$, ****: $0.0001 >$ p-value $>= 0$, no-significance (ns): p-value $>= 0.06$.

The results of the statistical test do not differ greatly between all the data and the data from the most common scan and the same significant differences can be observed between the same groups and measures.

3.2 Functional connectivity

From the given preprocessed rs-fMR images, we first extracted the intrinsic frequency per region. The intrinsic frequency per region per subject and group is shown in Figure 10.

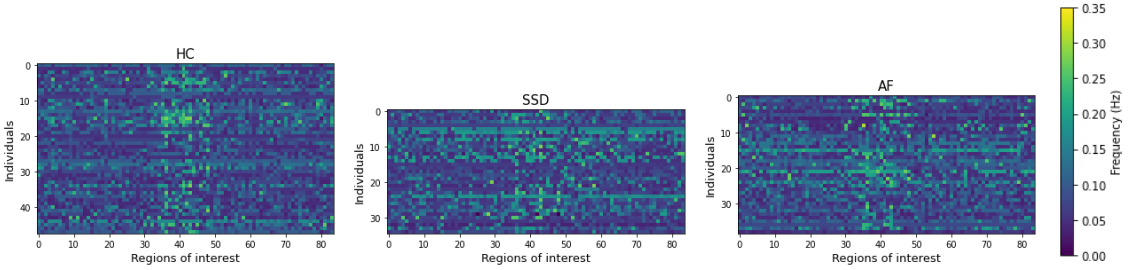

Figure 10: Intrinsic frequencies for each group.

A number of five simulations were performed, in five parallel tasks, and we tested twenty different G-values. The results were a BOLD time series and a functional connectivity matrix for each subject. An example can be seen in Figure 11.

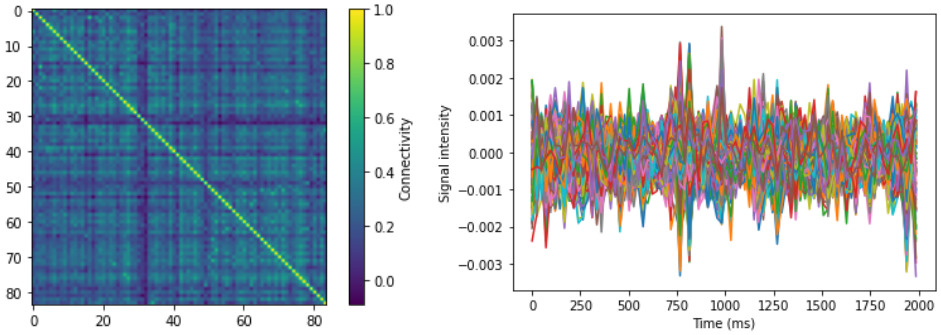

Figure 11: Result of simulations. Left: sFC of a healthy patient, at G = 5. Right: BOLD time series of the same patient with the same G, in which each colour represents a ROI.

With the obtained matrices, the Pearson correlation was performed against the experimental sFC, the correlation-G curves were approximated, and the desired value was computed. Some examples have been shown in Figure 5.

For the obtained G, correlation value and their ratio for each subject, the distribution of the three populations can be seen in Figure 12.

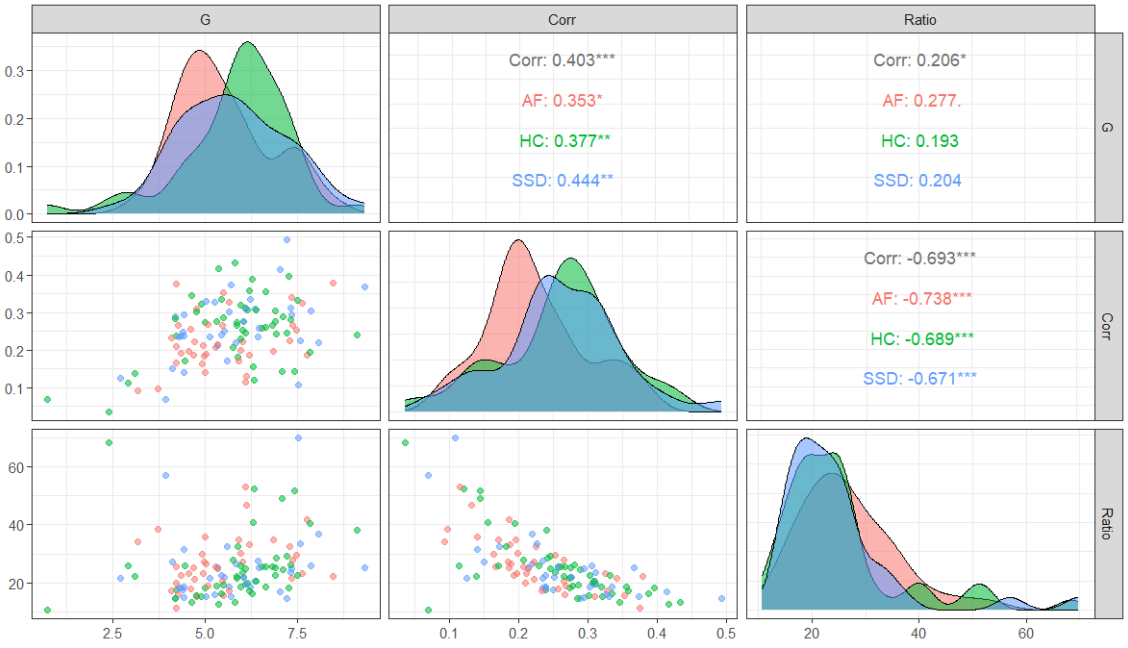

Figure 12: Distribution of populations.

As it does not follow a normal distribution, the Kruskal-Wallis test was applied to study the group differences for these parameters. The results of this study after FDR correction can be seen in Figure 13. Furthermore, the means and standard deviations and p-values for these measures can be observed in Table 4.

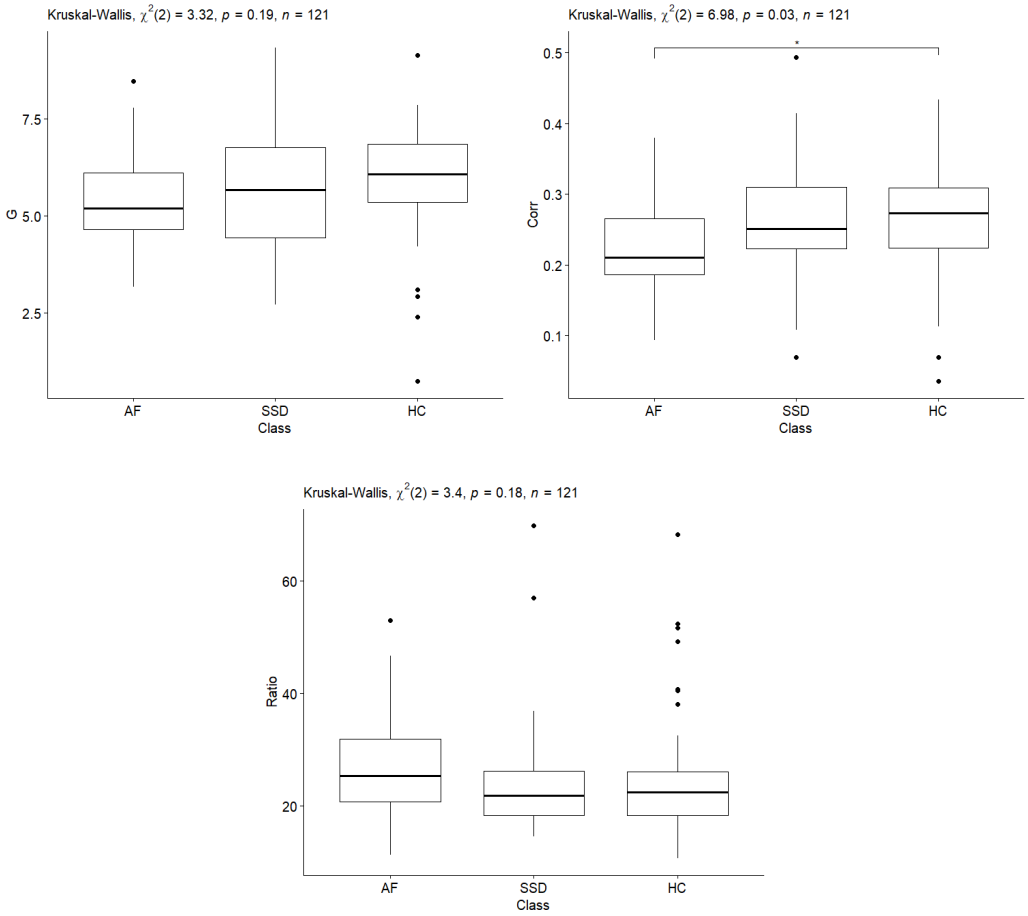

Figure 13: Parameters obtained during the Kruskal-Wallis test for each group for the functional connectivity study.

	HC	SSD	AF	p-value	Post hoc
G	5.86 (1.48)	5.80 (1.44)	5.51 (1.23)	0.19	ns
Corr	0.26 (0.09)	0.26 (0.09)	0.22 (0.07)	0.0305	AF<HC*
Ratio	25.19 (11.49)	24.63 (11.32)	26.69 (8.95)	0.183	ns

Table 4: For the results obtained in the statistical analysis of G, Pearson's correlation (Corr) and G/Corr (Ratio): mean and standard deviations for each group (HC, SSD and AF), p-value obtained for the Kruskal-Wallis test, and significance found after Dunn's post hoc test.
*: $0.06 >$ p-value $>= 0.01$, **: $0.01 >$ p-value $>= 0.001$, ***: $0.001 >$ p-value $>= 0.0001$, ****: $0.0001 >$ p-value $>= 0$, no-significance (ns): p-value $>= 0.06$.

The only significant difference within the studied measures appears in the Pearson correlation, between AF and SSD.

4 Discussion

4.1 Structural analysis

In the first analysis, we compared the topological properties of the structural connectivity between HC, AF, and SSD groups. In particular, we explored the global efficiency (EGLOB), the mean clustering coefficient (MCC), the characteristic path length (CPL), and small-worldness (SW). Our results suggest that there exists a significant difference in the EGLOB and MCC measures between groups, triggered by the AF group. Both EGLOB and MCC appeared to be significantly larger for AF patients with respect to HC, while SSD showed intermediate values. Moreover, CPL was also significantly larger in AF patients with respect to HC. However, we did not find any significant difference with respect to SW. All these measures might be partially related, as Figure 7 demonstrates, with correlations ranging from around [0.1,0.8], explaining slightly different perspectives of the problem at hand. A larger path length and clustering coefficient might appear as a consequence of a more pronounced network pruning for the AF patients when compared to SSD and especially HC. However, the fact that EGLOB is even larger in these patients, might indicate that such alterations are not necessarily associated with negative outcomes at these stages. Contrary to our initial hypotheses, we can state that these results might suggest the existence of substrate variations early on in the course of the disease.

Few authors had previously investigated structural connectivity topological properties of youth with a first episode of psychosis, divided by diagnosis at follow-up. Griffa and colleagues [27] reported an overall brain disconnectivity that was more pronounced in patients at the advanced stages of the first episode. They did not find any association between their findings and disease symptoms and severity, measured through PANSS and GAF scores respectively, nor with antipsychotic doses. However, they reported a negative association with processing speed, suggesting that such a disconnected state in the first episode might be impacting very concrete cognitive or clinical domains. The authors investigated structural connectivity in psychosis as a whole, while others specifically investigated this problem across specific psychotic diagnoses. In particular, Fernandes and colleagues [28] investigated the structural connectivity of pediatric patients with bipolar disorders, reporting only local topological differences with a tendency to correlate with specific clinical domains, such as IQ and affective psychotic symptoms. On the other hand, Ottet and colleagues [29] argued the difficulty in finding consistent structural variations in such a heterogeneous entity as schizophrenia, for which they suggested focusing on a homogeneous genetic variant known as 22q11.2 deletion syndrome in an adult and chronic sample. Similarly to what we reported for the AF group, they found an increased CPL but a preserved SW, while against our results, EGLOB appeared to be slightly decreased.

Overall, these studies show a certain overlap with our findings, potentially confirming the existence of dissimilar structural connectivity in AF patients with a first episode and in SSD patients at some point, when compared to HC. However, the populations studied, the experiments performed, the topological measures extracted, and the subsequent statistical analyses significantly differed across them, for which a direct

comparison and subsequent indubitable conclusion extraction is not possible. One of the main confusion sources might be the individual stage of maturation and disease, as work by Gri□a and colleagues [27] demonstrate, for which the association of these measures and topological extracted ones should be tested. A similar reasoning applies to antipsychotic medication and standardized or equivalent doses.

Of particular interest is our finding of a slightly increased EGLOB for patients when compared to HC, because of its counterintuitiveness, which cannot be contrasted with the literature because of all the aforementioned. Accounting for the individual stage of maturation and disease, but also antipsychotic equivalent doses, future work should focus on the statistical association of our results with specific clinical and cognitive domains, similarly to Fernandes and colleagues [28].

One potential confounding a□ecting our particular study was the scanner upgrade at the time of the acquisition. Even though it was the same scanner with a few upgrades, we repeated the experiments only for images obtained using the first scan, but not for the second one, as a very limited sample was available with a large imbalance between groups. This was performed to ensure that having obtained the images with two di□erent scans, with a class imbalance between them, did not significantly alter the results. Our results show that the di□erences in the measures are not altered substantially, and the same significant di□erences are presented in all cases except for MCC, in which a significant di□erence exists for SSD-HC, while for the whole set, a significant di□erence in MCC was present between SSD and AF. Therefore the extraction of the images from two di□erent scans should not be generating biased results.

In conclusion, in the first part of this bachelor's thesis (BT), we found a potential variation in the structural connectivity in psychotic patients, especially pronounced in the AF group. However, our results suggest that at the clinical and maturation stage of our group, under their ATP equivalent doses, these changes might not be negatively impacting the network e□ciency. Future studies should consider several covariates and associations to specific clinical domains while considering that only half of the story can be explained from these findings, for which the second part of this BT was conducted.

4.2 Simulations

In a second analysis, we investigated an approximation of the structural contribution in the experimental rs-fMRI, by modifying the G parameter of the Hopf-bifucation-based model [25]. When only modifying the G parameter, and comparing the sFC, we could observe that the resulting simulations barely changed from a specific G value, reaching a top performance in terms of similarity with the experimental rs-fMRI observations. Therefore, we assumed this minimum G was associated with the optimal value, while the correlation at that point was the peak correlation that could be reached only using individual structural information. Given the fact that G is associated with the contribution of the structural connectivity, as seen in section 2.4.1, and there is only another factor associated with the neurometabolic contribution that we kept constant (i.e., the bifurcation parameter), we assumed that

the correlation value was comparatively providing us with indirect information regarding neurometabolic contribution. We also normalized and investigated potential differences of a standardized version of G with respect to the peak correlation found.

From the three described measures, the only significant difference we found in this study was in the experimental-simulated sFC correlation measure, between AF and HC groups, where AF simulations reported significantly lower correlation with respect to HC ones. No other group comparison survived FDR correction.

These results, together with the fact that AF were the ones showing a larger variation in terms of structural connectivity might contrast with what our group previously reported [15] in a dynamic functional connectivity analysis. Particularly, the AF group displayed similar dynamic functional connectivity properties to the HC group, whereas SSD was the one that portrayed larger functional connectivity alterations. The authors specifically investigated measures associated with the temporal component of FC (i.e., easiness in the activation of different patterns, summarized by immobility, the metabolic cost of transitions, and efficiency in the activation of the whole repertoire), which might be related to specific clinical/cognitive domains, such as processing speed as found by Griffa and colleagues [27] for the structural alteration, but they could not prove it.

All these taken together could suggest that the AF group displays a greater neurometabolic contribution, that could serve as a compensatory mechanism for the structural differences, but further and deeper analyses are required to confirm such results.

4.3 Revisiting hypothesis: conclusions

According to our initial hypothesis, structural connectivity would have shown no differences between the three studied groups, while the higher contribution for the arising sFC signal of FEP would have corresponded to the neurometabolic contribution. However, we have found that this was not the case and that the groups had a significant difference with regard to the connectivity of their substrate, especially remarkable for the AF group. Moreover, our results suggest that AF may have a higher neurometabolic contribution when compared to HC, while no significant difference was found for SSD compared to HC or AF. According to the structural results, in which AF was the one with higher differences to the control group, and to the simulations, in which it showed a significant difference in the correlation, we hypothesize that this group may be experiencing compensatory mechanisms to the structural disconnection experienced. With regards to SSD, this group was the one that showed greater functional differences to the control group in [15], which our results seem to suggest that it may be caused by the structural difference experienced that does not seem to be compensated by a higher neurometabolic contribution.

4.4 Contribution and further work

The results of this study may help understand the cause-consequence relationships of the factors that may be giving rise to this condition and separate the effects on

AF and SSD FEP brains. Moreover, it can help suggest which changes are being produced in the brain at the early stages of the disease.

However, there are some limitations to this study, both regarding technical procedures and data used. An example is the validation of the obtained tractography, which has not been objectively and quantitatively performed in this study, although they were visually inspected and their resulting structural matrices were compared to expected results, accepting them whenever they seemed sensible. Moreover, even if there is already a noise correction applied in the preprocessing, a test could be performed to determine whether residual noise is a□ecting the results of the simulations, such as computing the correlation of the obtained measurements in the output of the simulations to movement parameters like framewise displacement.

Even if the results may be suggesting that there is a structural dominance in the prediction of the simulations, we have not fully tested the neurometabolic contribution in the patients. Therefore, the simulations should be also performed while modifying the bifurcation parameter. By studying this parameter, we could extract more robust conclusions on the phenomena being observed.

Another aspect to take into account is that, while we have computed the mean of the obtained sFC to make them more robust, this cannot be done in the experimental data, as there is only one time series per patient. However, sFC is more robust to noise than the dynamical alternative, therefore this should not a□ect the results in great measure.

Additionally, in further steps, it would be interesting to perform the structural connectivity analysis with measures or methods that allowed for the regional study of the perceived changes, to identify whether the disconnection lies in a particular area of the brain.

5 Additional information

Index	Region name
1, 50	Left and Right Banks of Superior Temporal Sulcus
2, 51	Left and Right Caudal Anterior Cingulate
3, 52	Left and Right Caudal Middle Frontal
4, 53	Left and Right Cuneus
5, 54	Left and Right Entorhinal
6, 55	Left and Right Fusiform
7, 56	Left and Right Inferior Parietal
8, 57	Left and Right Inferior Temporal
9, 58	Left and Right Isthmus
10, 59	Left and Right Lateral Occipital
11, 60	Left and Right Lateral Orbitofrontal
12, 61	Left and Right Lingual
13, 62	Left and Right Medial Orbitofrontal
14, 63	Left and Right Middle Temporal
15, 64	Left and Right Parahippocampal
16, 65	Left and Right Paracentral
17, 66	Left and Right Pars Opercularis
18, 67	Left and Right Pars Orbitalis
19, 68	Left and Right Pars Triangularis
20, 69	Left and Right Pericalcarine
21, 70	Left and Right Postcentral
22, 71	Left and Right Posterior Cingulate
23, 72	Left and Right Precentral
24, 73	Left and Right Precuneus
25, 74	Left and Right Rostral Anterior Cingulate
26, 75	Left and Right Rostral Middle Frontal
27, 76	Left and Right Superior Frontal
28, 77	Left and Right Superior Parietal
29, 78	Left and Right Superior Temporal
30, 79	Left and Right Supramarginal
31, 80	Left and Right Frontal Pole
32, 81	Left and Right Temporal Pole
33, 82	Left and Right Transverse Temporal
34, 83	Left and Right Insula
35, 84	Left and Right Cerebellum Cortex
36, 43	Left and Right Thalamus
37, 44	Left and Right Caudate
38, 45	Left and Right Putamen
39, 46	Left and Right Pallidum
40, 47	Left and Right Hippocampus
41, 48	Left and Right Amygdala
42, 49	Left and Right Accumbens area

Table A1: Regions of interest considered during the study.

Bibliography

[1] Matcheri S. Keshavan et al. "A dimensional approach to the psychosis spectrum between bipolar disorder and schizophrenia: The Schizo-Bipolar Scale". In: *Schizophrenia Research* 133 (1-3 Dec. 2011), pp. 250–254. ISSN: 09209964. DOI: 10.1016/j.schres.2011.09.005.

[2] Ellen Ji et al. "From the microscope to the magnet: Disconnection in schizophrenia and bipolar disorder". In: *Neuroscience Biobehavioral Reviews* 98 (Mar. 2019), pp. 47–57. ISSN: 0149-7634. DOI: 10.1016/J.NEUBIOREV.2019.01.005.

[3] K J Friston and C D Frith. "Schizophrenia: a disconnection syndrome?" In: *Clinical neuroscience (New York, N.Y.)* 3 (2 1995), pp. 89–97. ISSN: 1065-6766.

[4] Daniel R. Weinberger. "A connectionist approach to the prefrontal cortex". In: *The Journal of Neuropsychiatry and Clinical Neurosciences* 5 (3 Aug. 1993), pp. 241–253. ISSN: 0895-0172. DOI: 10.1176/jnp.5.3.241.

[5] Karl Friston et al. "The dysconnection hypothesis (2016)". In: *Schizophrenia Research* 176 (2-3 Oct. 2016), pp. 83–94. ISSN: 0920-9964. DOI: 10.1016/J.SCHRES.2016.07.014.

[6] Ruth Gallardo-Ruiz et al. "Long-Term Grey Matter Changes in First Episode Psychosis: A Systematic Review". In: *Psychiatry Investigation* 16 (5 May 2019), pp. 336–345. ISSN: 1738-3684. DOI: 10.30773/pi.2019.02.10.1.

[7] Dong-Min Yin et al. "Synaptic Dysfunction in Schizophrenia". In: 2012, pp. 493–516. DOI: 10.1007/978-3-7091-0932-8_22.

[8] K. E. Stephan, K. J. Friston, and C. D. Frith. "Dysconnection in Schizophrenia: From Abnormal Synaptic Plasticity to Failures of Self-monitoring". In: *Schizophrenia Bulletin* 35 (3 Mar. 2009), pp. 509–527. ISSN: 0586-7614. DOI: 10.1093/schbul/sbn176.

[9] João M.N. Duarte and Lijing Xin. "Magnetic Resonance Spectroscopy in Schizophrenia: Evidence for Glutamatergic Dysfunction and Impaired Energy Metabolism". In: *Neurochemical Research 2018 44:1* 44 (1 Apr. 2018), pp. 102–116. ISSN: 1573-6903. DOI: 10.1007/S11064-018-2521-Z. URL: https://link.springer.com/article/10.1007/s11064-018-2521-z.

[10] Gisela Sugranyes et al. "Gray Matter Volume Decrease Distinguishes Schizophrenia From Bipolar O□spring During Childhood and Adolescence". In: *Journal of the American Academy of Child Adolescent Psychiatry* 54 (8 Aug. 2015), 677–684.e2. ISSN: 08908567. DOI: 10.1016/j.jaac.2015.05.003.

[11] Gisela Sugranyes et al. "Clinical, Cognitive, and Neuroimaging Evidence of a Neurodevelopmental Continuum in O□spring of Probands With Schizophrenia and Bipolar Disorder". In: *Schizophrenia Bulletin* 43 (6 Oct. 2017), pp. 1208–1219. ISSN: 0586-7614. DOI: 10.1093/schbul/sbx002.

[12] S. Marques et al. "First-episode psychosis: What does it mean?" In: *European Psychiatry* 33 (S1 Mar. 2016), s258–s258. ISSN: 0924-9338. DOI: 10.1016/j.eurpsy.2016.01.656.

[13] P. B. Jones. "Adult mental health disorders and their age at onset". In: *British Journal of Psychiatry* 202 (s54 Jan. 2013), s5–s10. ISSN: 0007-1250. DOI: 10.1192/bjp.bp.112.119164.

[14] Pilar de Castro-Manglano et al. “Structural brain abnormalities in first-episode psychosis: di□erences between a□ective psychoses and schizophrenia and relationship to clinical outcome”. In: *Bipolar Disorders* 13 (5-6 Aug. 2011), pp. 545–555. ISSN: 13985647. DOI: 10.1111/j.1399-5618.2011.00953.x.

[15] Mireia Masias et al. “Altered temporal dynamics of resting-state fMRI in adolescent-onset first-episode psychosis”. 3002In press.

[16] *Enhancing Neuro Imaging Genetics Through Meta Analysis (ENIGMA)*. URL: https://enigma.ini.usc.edu/.

[17] Mark W. Woolrich et al. “Bayesian analysis of neuroimaging data in FSL”. In: *NeuroImage* 45 (1 Mar. 2009), S173–S186. ISSN: 10538119. DOI: 10.1016/j.neuroimage.2008.10.055.

[18] Nicholas J Tustison et al. “The ANTsX ecosystem for quantitative biological and medical imaging.” In: *Scientific reports* 11 (1 Apr. 2021), p. 9068. ISSN: 2045-2322. DOI: 10.1038/s41598-021-87564-6.

[19] Brian B Avants et al. “The pediatric template of brain perfusion”. In: *Scientific Data* 2 (1 Feb. 2015), p. 150003. ISSN: 2052-4463. DOI: 10.1038/sdata.2015.3.

[20] J-Donald Tournier et al. “MRtrix3: A fast, flexible and open software framework for medical image processing and visualisation”. In: *NeuroImage* 202 (Nov. 2019), p. 116137. ISSN: 10538119. DOI: 10.1016/j.neuroimage.2019.116137.

[21] Tabinda Sarwar, Kotagiri Ramamohanarao, and Andrew Zalesky. “Mapping connectomes with di□usion MRI: deterministic or probabilistic tractography?” In: *Magnetic Resonance in Medicine* 81 (2 Feb. 2019), pp. 1368–1384. ISSN: 0740-3194. DOI: 10.1002/mrm.27471.

[22] Mikail Rubinov and Olaf Sporns. “Complex network measures of brain connectivity: Uses and interpretations”. In: *NeuroImage* 52 (3 Sept. 2010), pp. 1059–1069. ISSN: 10538119. DOI: 10.1016/j.neuroimage.2009.10.003.

[23] Tonya White and Vince D Calhoun. “Dissecting Static and Dynamic Functional Connectivity: Example From the Autism Spectrum.” In: *Journal of experimental neuroscience* 13 (2019), p. 1179069519851809. ISSN: 1179-0695. DOI: 10.1177/1179069519851809.

[24] Jonathan D. Power, Bradley L. Schlaggar, and Steven E. Petersen. “Recent progress and outstanding issues in motion correction in resting state fMRI”. In: *NeuroImage* 105 (2015), pp. 536–551. DOI: 10.1016/j.neuroimage.2014.10.044.

[25] Gustavo Deco et al. “The dynamics of resting fluctuations in the brain: metastability and its dynamical cortical core”. In: *Scientific Reports* 7 (1 June 2017), p. 3095. ISSN: 2045-2322. DOI: 10.1038/s41598-017-03073-5.

[26] Frank Freyer et al. “Biophysical Mechanisms of Multistability in Resting-State Cortical Rhythms”. In: *The Journal of Neuroscience* 31 (17 Apr. 2011), pp. 6353–6361. ISSN: 0270-6474. DOI: 10.1523/JNEUROSCI.6693-10.2011.

[27] Alessandra Gri□a et al. “Brain connectivity alterations in early psychosis: from clinical to neuroimaging staging.” In: *Translational psychiatry* 9 (1 Feb. 2019), p. 62. ISSN: 2158-3188. DOI: 10.1038/s41398-019-0392-y.

[28] Henrique M. Fernandes et al. “Disrupted brain structural connectivity in Pediatric Bipolar Disorder with psychosis”. In: *Scientific Reports* 9 (1 Sept. 2019), p. 13638. ISSN: 2045-2322. DOI: 10.1038/s41598-019-50093-4.

[29] Marie-Christine Ottet et al. “Graph theory reveals dysconnected hubs in 22q11DS and altered nodal e□ciency in patients with hallucinations.” In: *Frontiers in human neuroscience* 7 (2013), p. 402. ISSN: 1662-5161. DOI: 10.3389/fnhum.2013.00402.